nature communications

Article

https://doi.org/10.1038/s41467-026-70491-3

Complete inhibition of β-tryptase by tetramer dissociation and active site allostery due to a single antibody residue

Received: 30 May 2025

Accepted: 27 February 2026

Published online: 09 April 2026

Check for updates

Henry R. Maun[1,6] ✉, Caleigh M. Azumaya[2,6], Benjamin T. Walters[2,3], Rajesh Vij[4], Ashley Morando[3,5], Kelly M. Loyet[3], James T. Koerber[4], Alexis Rohou[2] & Robert A. Lazarus[1] ✉

Human β-tryptase, a tetrameric trypsin-like serine protease, is an important mediator of inflammatory responses in asthma, allergy and other diseases. Here we report an anti-β-tryptase antibody with a superior mechanism of action compared to others since it not only inhibits tetrameric β-tryptase, but also completely inhibits monomeric β-tryptase activity. The antibody binds to an exosite that causes tetramer dissociation as either an IgG or Fab and, in addition, allosterically alters the substrate binding cleft on monomers, thus preventing substrate binding and proteolysis. We solve the cryoEM structure of the complex, generate biochemical data and engineer point mutations to elucidate the allosteric path of inhibition. This ultimately reveals a single Asp to Gly mutation in CDR-L3 that only slightly impacts binding affinity, but completely eliminates inhibitory activity. Finally, we improve antibody inhibitory potency up to 4.7-fold by structure-based design creating new charge-charge interactions. This antibody may have enhanced efficacy and potential to assess the relevance of β-tryptase, including monomers, in biological and clinical settings.

Mast cells play an important role in inflammation and host defense in response to foreign stimuli such as allergens, bacteria, viruses, and venoms and have also been implicated in a number of diseases including asthma, anaphylaxis, inflammatory bowel disease, and atherosclerosis[1–3]. IgE crosslinking on the surface of mast cells, through antigens or allergens, induces the release of secretory granules that contain histamine, heparin, cytokines, chemokines as well as high levels of various proteases[1,4], in particular β-tryptase[5]. In the respiratory tract, this rapid secretion of active proteases has many physiological consequences such as increased collagen production by lung fibroblasts and proliferation and contraction of lung smooth muscle cells, specifically in type 2-low inflammation and type 2-low asthma[6–10]. Thus, potent and specific inhibitors of mast cell proteases may have broad therapeutic potential for diseases driven by excessive mast cell activation[4,11], given that they do not impair their vital 'normal' physiological functions.

β-tryptase, a trypsin fold serine protease belonging to the S1A subfamily of S1 proteases (MEROPS peptidase database)[12], is the most abundant protease stored in mast cell granules. Upon pro-peptide cleavage by cathepsin C[13], β-tryptase forms tetramers in mast cell granules, which are stabilized by binding to serglycin proteoglycans carrying heparin glycosaminoglycan[14]. Extracellular β-tryptase monomers have often been considered to be inactive under physiological conditions[15–18], but we and others have shown that monomeric tryptase can, in fact, retain activity in vitro at high heparin concentrations, since heparin also acts as a cofactor that increases activity[18–22]. The findings

[1]Department of Early Discovery Biochemistry, Genentech, Inc., South San Francisco, CA, USA. [2]Department of Structural Biology, Genentech, Inc., South San Francisco, CA, USA. [3]Department of Biochemical and Cellular Pharmacology, Genentech, Inc., South San Francisco, CA, USA. [4]Department of Antibody Engineering, Genentech, Inc., South San Francisco, CA, USA. [5]Present address: 4D Molecular Therapeutics, Emeryville, CA, USA. [6]These authors contributed equally: Henry R. Maun, Caleigh M. Azumaya. ✉e-mail: maun.henry@gene.com; lazarus.bob@gene.com

Table 1 | Binding affinity and kinetics of monomeric β-tryptase binding to E82.AS anti-β-tryptase variants measured by surface plasmon resonance (SPR)

Analyte: zymogen βI-tryptase	Ligand Level (RU)	Rmax (RU)	K_D (M)	k_a ($M^{-1}•s^{-1}$)	k_d (s^{-1})	Chi² (RU^2)
E82.AS WT	187.6	69.3	6.71×10^{-11}	1.88×10^{6}	1.26×10^{-4}	7.49
E82.AS LC-WT HC.S30K.Y31K	222.6	77.2	4.46×10^{-11}	2.00×10^{6}	8.93×10^{-5}	0.536
E82.AS LC-WT HC.S30R.Y31R	230.7	83.5	7.41×10^{-11}	1.49×10^{6}	1.10×10^{-4}	0.698
E82.AS LC.D93G. HC.WT	188.7	68.4	7.88×10^{-10}	3.40×10^{5}	2.68×10^{-4}	3.24
E82.AS LC.D93G. HC.S30K.Y31K	221.5	74.2	5.04×10^{-10}	5.07×10^{5}	2.56×10^{-4}	0.505
E82.AS LC.D93G HC.S30R.Y31R	224.8	81.4	6.71×10^{-10}	3.96×10^{5}	2.66×10^{-4}	1.01

E82.AS IgG variants were immobilized on a sensor chip via an anti-human Fc capture antibody and binding kinetics were measured and determined by injection of monomeric zymogen βI-tryptase.

of the antibody we present herein provide a future opportunity to address the precise effect of heparin on monomeric tryptase activity in vivo, which is otherwise difficult to determine. Proteolytically active β-tryptase tetramers stimulate a range of inflammatory and tissue remodeling processes through cleavage of a variety of substrates including proteinase-activated receptor (PAR-2)[7], vasoactive intestinal peptide (VIP)[23], matrix metalloproteinases (MMPs)[22,24], fibronectin, and collagen[8], but in some cases, cleavage can also lead to inhibition of biological pathways[25–27].

The crystal structures of active human β-tryptase show a frame-like, toroidal quaternary structure with a quasi 2-fold symmetry among the four individual protomers, surrounding a central pore with the four active sites facing toward the pore[28,29]. Positively charged surfaces outside the pore have been implicated in heparin binding that stabilizes the tetramer[18,30]. Due to the dimensions of the pore entrance (15 × 40 Å), access to the four active sites is limited to small peptide substrates and loops from larger proteins that are flexible enough to enter the pore. Common endogenous inhibitors of trypsin-like proteases such as alpha 1-antitrypsin, alpha 2-macroglobulin or Kunitz domain containing proteins are too large to access the active sites through the pore[31,32]. Only a small number of β-tryptase inhibitors in nature have been described, which include tick-derived protease inhibitor (TdPI)[33], leech-derived tryptase inhibitor (LDTI)[34,35], peptide leucine arginine (pLR)[36] and cyclotheonamide E4[37]. Engineered peptides derived from the cystine-knot peptides EETI-II[38] and MCoTI-II[39,40] as well as Bowman-Birk inhibitor peptides[41] have been reported as potent β-tryptase inhibitors, but these molecules are not selective for β-tryptase and can block other trypsin-like serine proteases as well. Small molecule active site inhibitors of β-tryptase have also been described in the literature[42–45] and some have shown therapeutic effects in guinea pig and sheep asthma models[46,47] and in humans[48], however, insufficient oral bioavailability, selectivity and/or tolerability have impeded further drug development efforts.

Inhibitory antibodies with drug-like properties and high specificity against their respective proteases can inhibit by either directly blocking the active site or indirectly modulating proteolytic activity via an allosteric mechanism[49]. We have previously described two inhibitory anti-β-tryptase antibodies with almost identical tryptase binding epitopes, that inhibit enzymatic activity allosterically by dissociating the active tetramer into monomers that are inactive at low heparin concentrations[10,50]. While these antibodies[10,50] had promising activities in vitro and one was investigated in human clinical trials[51], an antibody that completely inhibits both tetrameric and monomeric tryptase and can be used as a Fab or scFv may lead to the successful development of a therapeutic in the clinic. A lower MW inhibitor may increase the likelihood of reaching clinically relevant concentrations in the lower airway, a limiting factor in previous tryptase clinical trials[51].

Here, we describe the mechanism of action (MOA) of an inhibitory anti-β-tryptase antibody (E82.AS). To the best of our knowledge, it binds to a previously unknown exosite, i.e., a binding site that is distinct from the 'active site', discovered by employing a series of biochemical, biophysical and structural biology experiments. We used hydrogen deuterium exchange mass spectrometry (HDX-MS) and cryogenic electron microscopy (cryoEM) to determine the β-tryptase:Fab interactions and discovered that E82.AS binding to an exosite changes the conformation of the active site cleft such that tryptase can no longer bind to substrates or active site inhibitors. Both the bivalent E82.AS IgG and the monovalent Fab dissociate tetrameric β-tryptase into completely inhibited monomers, even at high heparin concentrations. Based on structure-guided design, we introduced two mutations in the first complementarity-determining region (CDR) of the heavy chain (HC), CDR-H1, that improved the inhibitory potency of the antibody 4.7-fold.

Notably, we identified a single residue mutation—D93G in CDR-L3 of E82.AS—that has relatively little effect on β-tryptase binding, but no longer dissociates the tetramers into monomers nor has any inhibitory effect on enzymatic activity. This is a rare finding. Our high-resolution structure of the complex allowed us to trace structural changes stemming from the interaction of E82.AS D93 with the exosite on the β-tryptase surface and observe the allosteric path of tryptase inhibition into the active site in molecular detail. Insights into the path of allosteric inhibition may be applicable to inhibitor designs of other trypsin-like serine proteases, where a high degree of specificity and potency is required for therapeutic intervention.

Results

Rabbit immunization with recombinant β-tryptase and subsequent monoclonal antibody development by standard hybridoma technology resulted in a small number of specific anti-β-tryptase antibodies that also showed potent inhibition of tetrameric tryptase[10]. In this paper, tryptase or β-tryptase refers to the βI-tryptase subtype, which was used herein to generate all data. One of the antibody clones, E82.AS, a human chimeric IgG1 antibody, bound to β-tryptase with very high affinity, having a $K_D = 67$ pM as measured by surface plasmon resonance (SPR) (Table 1). Both chimeric IgG and Fab E82.AS showed dose-dependent inhibition of tetrameric β-tryptase in a chromogenic enzyme activity assay containing 1 μg/mL heparin (Fig. 1a), having IC_{50} values of 47 nM and 86 nM, respectively. Epitope binning analysis of E82.AS using biolayer interferometry demonstrated that E82.AS did not compete with previously described inhibitory anti-βI-tryptase antibodies 31A.v11[10] and E104.v2[50] (Supplementary Fig. 1). Both of these antibodies are structurally and mechanistically well understood, having very different MOAs, yet highly overlapping binding epitopes. This indicates that E82.AS binds to a distinct epitope on β-tryptase and interaction with this epitope is sufficient to inhibit enzymatic activity.

In order to determine whether the mechanism of β-tryptase inhibition by E82.AS is driven by tetramer dissociation into monomers, as found with 31A.v11 and E104.v2, we formed complexes of human β-tryptase tetramers with Fab E82.AS in the absence of heparin and analyzed them by size exclusion chromatography (SEC) and SDS-PAGE (Fig. 1b, c). β-tryptase tetramers mixed with excess Fab E82.AS eluted as a complex of both components with a retention volume of 14 mL

https://doi.org/10.1038/s41467-026-70491-3

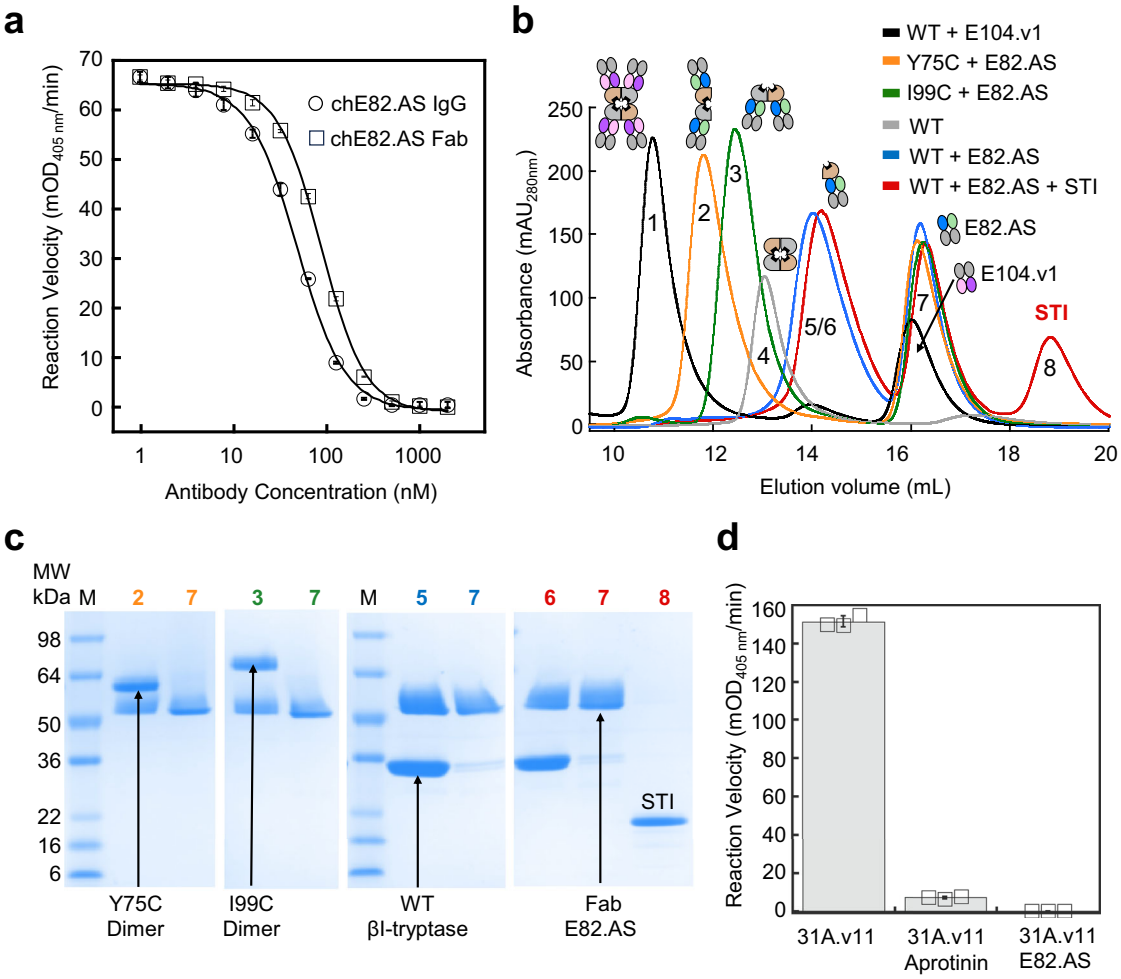

Fig. 1 | Interaction of antibody E82.AS with β-tryptase. a Rabbit-human chimeric anti-β-tryptase antibody E82.AS inhibits β-tryptase in a chromogenic enzyme activity assay. Concentration-dependent inhibition of 1 nM βI-tryptase enzymatic activity by E82.AS IgG1 and Fab E82.AS in TNH1 buffer with IC_{50} values of 47 nM and 86 nM, respectively. Data is represented as mean ± s.d. ($n = 3$ independent experiments). **b** Analysis of complex formation by SEC of Fab E82.AS with tetrameric β-tryptase (WT (in the presence (red) and absence (blue) of soybean trypsin inhibitor (STI)), Y75C (orange) and I99C (green) mutants) in the absence of heparin as well as WT tetramer alone (gray) and in complex with E104.v1 (black) as controls, all in SEC buffer. Elution volumes of the marked peaks 1–9 are: Peak 1 = 10.4 mL, Peak 2 = 11.8 mL, Peak 3 = 12.5 mL, Peak 4 = 13 mL, Peak 5/6 = 14 mL, Peak 7 = 16 mL (excess Fabs E82.AS and E104.v1, respectively) and Peak 8 = 18.8 mL, which represents excess STI. Chromatograms show representative results from two independent experiments for each chromatogram. **c** SDS-PAGE of β-tryptase complexes from SEC fractions. SDS-PAGE analysis of the eluting proteins from **b** from the middle of the peaks 2, 3, 5, 6, 7, 8; M refers to MW markers. The peak numbers are color-coded according to **b** legend. Gels show representative results from two independent experiments. **d** Inhibition of residual enzymatic activity of WT β-tryptase monomers bound to IgG1 31A.v11 in the presence of heparin. IgG1 E82.AS (1 μM) and aprotinin (2 μM) were added after tetrameric β-tryptase (100 nM) was dissociated into monomers by IgG1 31A.v11 (1 μM) in TNH100 buffer. Data is represented as mean ± s.d. ($n = 3$ independent experiments). Source data are provided as a Source Data file.

(blue trace, Fig. 1b). This complex elutes with a larger volume than tetrameric tryptase alone (13 mL, gray trace Fig. 1b) and is indicative of tryptase monomers bound to Fab (lower molecular weight than tetramers), showing that Fab E82.AS binding to tetrameric β-tryptase dissociates tetramers into monomers.

We then tested whether Fab E82.AS causes β-tryptase tetramer dissociation via destabilization of the small interface or the large interface of the β-tryptase tetramer. To do this, we used previously described β-tryptase tetramer mutants Y75C and I99C (chymotrypsinogen numbering[52] used throughout for β-tryptase), where the tetramers are covalently locked at their small (Y75C) or large (I99C) protomer interfaces by disulfide bonds and can only dissociate into dimers[19]. Complexes of these mutants bound to Fab E82.AS were analyzed by SEC and SDS-PAGE. Both tetramer mutants, Y75C and I99C, when bound to Fab E82.AS, formed complexes with retention volumes of 11.8 mL and 12.5 mL, respectively (orange and green traces, Fig. 1b), larger than the retention volume of 10.4 mL observed for tetrameric β-tryptase bound to 4 Fabs of E104.v1[50]. This indicates that Fab E82.AS binding to tetrameric β-tryptase destabilizes both the small and the large protomer interfaces. Note that while E104.v1 and E104.v2 have identical CDR sequences and K_D values of 0.5 nM for βI-tryptase monomer, they differ at two key Vernier residues (V71R and F78V), which resulted in destabilization of the small interface by E104.v2, but not by E104.v1[50].

We wondered whether the inhibition of β-tryptase catalytic activity by E82.AS was entirely attributable to its ability to dissociate tryptase tetramers. To test this, we compared E82.AS with another antibody, 31A.v11, which also dissociates tetramers, but neither alters the active site conformation of tryptase monomers[10] when compared to tetramer[28] (RMSD 0.53 Å) nor inhibits the residual enzymatic activity of the resulting tryptase monomers (Supplementary Fig. 2). Upon addition of excess active site inhibitor aprotinin (2 μM), this residual enzymatic activity from 31A.v11-bound tryptase was inhibited by 95.3% (Fig. 1d), still retaining some residual activity. Notably, when we added

Fab E82.AS (1 μM) to 31A.v11-bound tryptase instead of aprotinin, we did not observe any detectable residual enzymatic activity (Fig. 1d). This suggests that in addition to tetramer dissociation, Fab E82.AS binding has an allosteric effect on the substrate binding site. To further examine this, we incubated a mixture of WT tetrameric β-tryptase and excess Fab E82.AS with the macromolecular active site inhibitor soybean trypsin inhibitor (STI). This resulted in a complex consisting of monomeric tryptase bound to Fab E82.AS, but which, importantly and unlike inhibitory antibody 31A.v11[10], did not include STI, as shown by SEC and SDS PAGE analysis (red trace, Fig. 1b, c). Both experiments suggest that E82.AS-bound β-tryptase has an altered active site conformation, which is incompatible with binding of the macromolecular active site inhibitor STI binding or with proteolytic cleavage of a small chromogenic substrate.

Next, we sought to elucidate the Fab E82.AS binding epitope on WT β-tryptase. We conducted HDX-MS experiments with β-tryptase alone or in complex with Fab E82.AS. Amide protons in β-tryptase with slower exchange rates in the presence of E82.AS indicated that structural dynamics in these regions were affected upon Fab binding. We identified a number of peptides whose amide protons exchanged significantly slower compared to β-tryptase alone and calculated the individual protection factors for the respective amino acid positions. The highest positive protection factors (PF), which indicate slower HDX, clustered at residues I162 through A183, T186 through G196, and A213 through V223 (chymotrypsinogen numbering[52]) (ΔPF between 1 and 1.7). Many of these residues (180 s loop and 220 s loop) are part of the surface exposed activation domain loops that change conformation upon transition from zymogen to enzyme conformation. Furthermore, positive protections factors for residues D189, G193 and S195, which are part of the S1 specificity pocket and the oxyanion hole, both vital for catalysis, suggest structural changes in the active site. Residues 169-173d and 221-224 form a continuous surface near the large protomer interface, which is the most likely binding epitope of E82.AS (Supplementary Fig. 3). Consistent with the epitope binning results, this main cluster of residues does not overlap with the binding epitopes of 31A.v11[10] or E104 (v1 or v2)[50]. All βI-tryptase residues with their respective calculated protection factors (log10 (ΔPF)) that represented slower or faster HDX in their amide bonds are listed in Supplementary Data 1.

While these experiments identified the likely epitope of E82.AS, the molecular details remained unclear as to how E82.AS dissociates tetramers into monomers and inhibits residual monomeric β-tryptase activity. This prompted us to employ cryoEM to gain high-resolution structural insights into the binding epitope of E82.AS as well as structural changes that occur in β-tryptase upon E82.AS binding. We formed a quaternary complex of WT β-tryptase, Fab E104.v2, Fab E82.AS with 3 mutations (K145E, E143S and Q199A in the kappa light chain) and an anti-kappa nanobody (Nb)[53]. The three mutations in the light chain (LC) of E82.AS abrogated anti-kappa Nb binding, ensuring that the Nb would only bind Fab E104.v2. Fab E104.v2 and the anti-kappa LC binding Nb were used as fiducial markers, increasing particle size and adding rigid features to aid in particle image alignment. This resulted in a structure at 3 Å global resolution with higher resolution at the Fab:β-tryptase interfaces (Fig. 2a, Supplementary Figs. 4 and 5, Supplementary Table 1). Consistent with the HDX-MS results, cryoEM data revealed that E82.AS binds to parts of the 170 s loop, the preceding 160 s helix and the 220 s loop (Fig. 2b). The antibody paratope is characterized by contributions from the LC (49% buried surface area) and the HC (64% buried surface area) with overall buried surface area of 764 Å^2 on β-tryptase. Antibody residues within 4 Å of β-tryptase are from CDR-L1 (V29, Y32), CDR-L3 (D92 to I95d), CDR-H2 (Y53, G54, S56), and CDR-H3 (F95, Y97, P98, A100) (Supplementary Fig. 6a). In β-tryptase, the epitope residues P132, G133, P161, M163, H166, I167, D169, A170, K171, H173, L173a, G173b, A173c, Y173d, N223, and R224 (chymotrypsinogen numbering[52]) are within 4 Å of E82.AS (Supplementary Fig. 6b). The same residues, except for P132 and G133 have ΔPF > 1, which is consistent with being part of the E82.AS binding epitope.

When we compared the Cα backbone of a β-tryptase protomer from the tetramer to the E82.AS-bound tryptase monomer, we discovered several significant conformational differences in the following areas: H36 to Y37b, G60 to D60e, R69 to Q81, Y173d to V173i, G184 to D194 and G216 to R224 (RMSD of the Cα backbone is 2.31 Å) (Fig. 2c). Furthermore, we cannot trace the Cα backbone in E82.AS-bound β-tryptase from I16 to K26 and W141 to K156 due to conformational heterogeneity (Fig. 2c). These findings have significant consequences for the active site and thus enzyme activity. Specifically, the oxyanion hole, which is critical for catalyzing proteolysis was non-existent due to a 4.6 Å shift of the main chain nitrogen atom of G193. Furthermore, the salt bridge interaction between D194 and the N-terminal primary amine of I16 was also non-existent, because the side chain of D194 was turned away by 90 degrees and thus the activation domain pocket was unavailable for stable N-terminal insertion (Fig. 2d). Finally, D189, which constitutes the important negative charge at the bottom of the S1 specificity pocket that interacts with positively charged P1 residues (Arg, Lys) of substrates, has moved away from the pocket; the distance between the two D189 Cβ atoms is 7.4 Å (Fig. 2e). Notably, catalytic triad residues H57, D102 and S195 were in similar positions (0.51 Å RMSD) compared to catalytically-competent β-tryptase. We provide a movie (Supplementary Movie 1) that allows a dynamic comparison of an 'active' β-tryptase protomer with a small molecule in the S1 pocket with an 'inactive' β-tryptase monomer bound to E82.AS. This movie shows the transition from the active enzyme conformation to a computational model of the 'zymogen-like' conformation upon E82.AS binding. The conformational changes for the N-terminus (I16), and residues D194, D189 and N223 are readily apparent.

Relative to the structure of tetrameric tryptase, we observed conformational changes from G60-D60e and R69-Q81 as well as structural heterogeneity from W141 to K156. These residues are at the small tetramer interface, which indicated increased dynamics in these regions of the protein compared to when they are part of the tetramer and have a defined structure for proper protomer interaction (Supplementary Fig. 7). It is difficult to conclude from this observation alone whether these conformational changes are directly induced by E82.AS binding or are due to the removal of stabilizing contacts to an adjacent monomer in the tetrameric state. Additionally, we observed conformational changes in β-tryptase at the E82.AS binding epitope near the large tetramer interface that could contribute to destabilization of this protomer-protomer interaction. D173g shifted by 5 Å and Y173d, which binds to a hydrophobic pocket in the neighboring tryptase protomer in the tetramer, rotated away from this pocket (Supplementary Fig. 8). The apparent destabilization of tetramers at both the large and small interfaces is a preferred MOA of E82.AS from the previously described inhibitory antibody E104.v2 that only destabilizes the small interface[50].

Since S30 and Y31 from the HC of E82.AS were in close proximity to a negatively-charged patch on β-tryptase created by D169, D173g and D173h (Fig. 3a), we thought we might be able to engineer energetically favorable electrostatic interactions by introducing positively-charged amino acids at these positions. Indeed, HC.S30K.Y31K and HC.S30R.Y31R improved potency by 3.4-fold and 4.7-fold compared to WT, respectively (WT E82.AS IC_{50} = 64.2 nM; HC.S30K.Y31K IC_{50} = 18.8 nM; HC.S30R.Y31R E82.AS IC_{50} = 13.7 nM) (Fig. 3b), although we did not see an improvement in affinity to tryptase as measured by SPR (Table 1).

Next, we wanted to determine how E82.AS leads to tetramer dissociation and allosterically affects the active site. We inspected the binding epitope and noticed that D93 in CDR-L3 points directly

https://doi.org/10.1038/s41467-026-70491-3

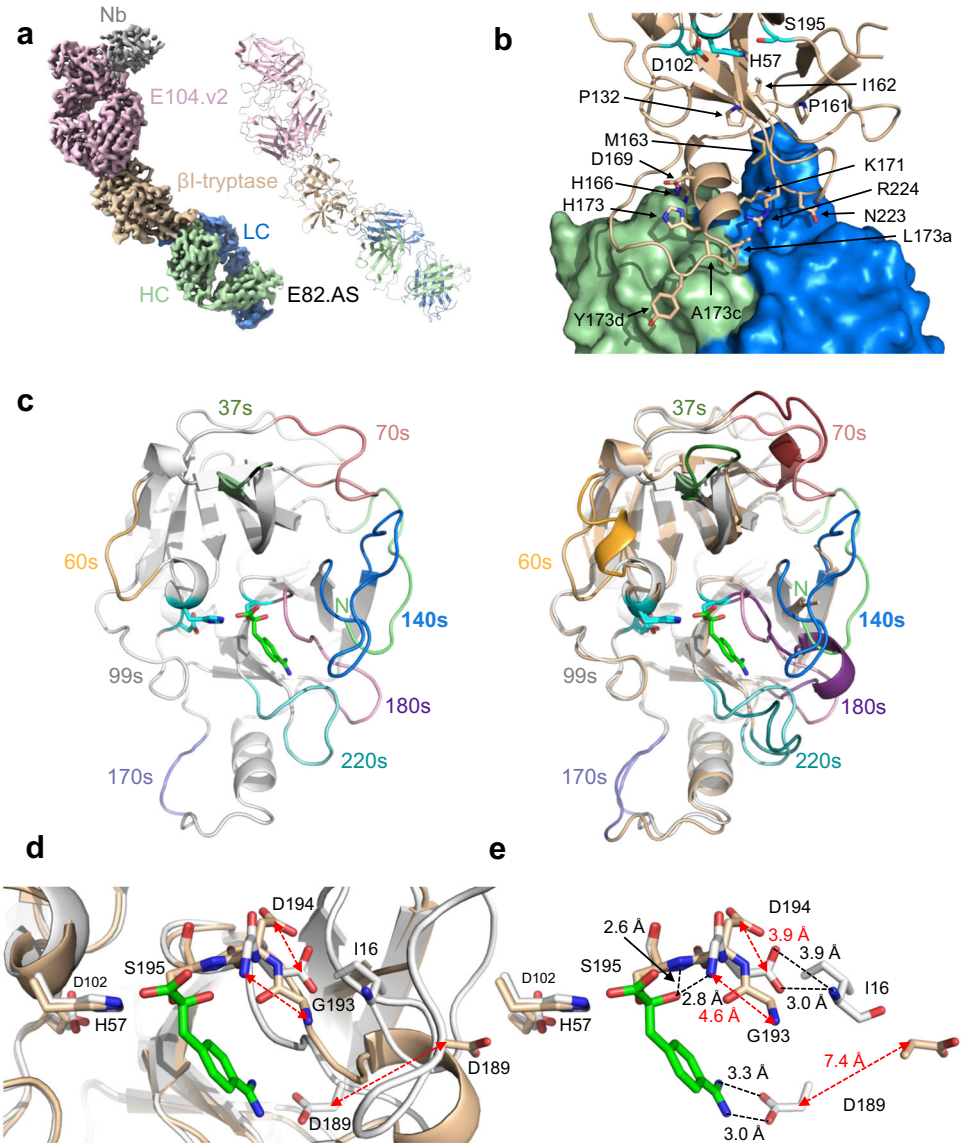

Fig. 2 | CryoEM structure at 3 Å of monomeric β-tryptase bound to Fab E82.AS. **a** CryoEM map of the E82.AS:βI-tryptase:E104.v2:Nb complex is shown in the left image. Cartoon representation of E82.AS:βI-tryptase:E104.v2 is shown in the right image. βI-Tryptase monomer is beige, light chain of E82.AS is blue, heavy chain of E82.AS is light green and E104.v2 is pink. The structure of the V_HH nanobody (Nb) in gray, which served as a fiducial marker, was rigid fit into the density from the crystal structure PDB: 6ANA. **b** Interactions of β-tryptase residues with LC and HC of Fab E82.AS. βI-Tryptase (beige) residues within 4 Å of E82.AS are shown in sticks. Catalytic triad residues are shown as cyan sticks. The E82.AS light chain and heavy are shown in blue and light green, respectively (surface representation). **c** Conformational differences in WT β-tryptase (a protomer from the tetramer) and E82.AS-bound β-tryptase (monomer). The eight surface loops and the N-terminal activation loop are labeled and shown in different colors in lighter shades for the tryptase protomer from tetrameric βI-tryptase (gray, PDB: 1A0L) (left panel). β-tryptase bound to E82.AS (beige) was structurally aligned with the protomer from 1A0L, which has an RMSD of 2.31 Å for the Cα backbone (right panel). Loops of the E82.AS-bound β-tryptase are colored in darker shades; no density was observed for the N-terminal activation loop (I16 - S25), the 140 s loop (G142 – P154). The covalent orthosteric small molecule active site inhibitor 4-amidinophenyl pyruvic acid (green) from 1A0L is shown as sticks to highlight the oxyanion hole and S1 specificity pocket. **d**–**e** Rearrangements of I16, D189, G193 and D194 disrupt the β-tryptase active site without perturbing the catalytic triad. Active site βI-tryptase from tetramer (gray) and βI-tryptase bound to E82.AS (beige) are structurally aligned and shown in cartoon; 4-amidinophenyl pyruvic acid (green) from 1A0L is shown as in Fig. 2c. Key β-tryptase residues I16, D189, G193 and D194 as well as catalytic triad residues are shown in sticks. Dashed lines refer to distances in Å between atoms where indicated; red dashes with arrows highlight major conformational changes.

towards the 220 s loop of β-tryptase. In the E82.AS-bound structure, N223 is displaced by 4.5 Å relative to its position in the unbound tetrameric structure due to steric hindrance by the side chain of LC.D93 (Fig. 4a). To test whether this distortion of the 220 s loop by LC.D93 leads to tetramer dissociation into monomers, we made a LC.D93G mutant, which eliminates the side chain, predicting that it would relieve the steric distortion of the 220 s loop. Indeed, the E82.AS LC.D93G mutant still bound β-tryptase with very high affinity as determined by SPR (E82.AS LC.D93G K_D = 788 pM) (Table 1). However, notably, this single point mutant no longer inhibited β-tryptase activity (Fig. 4b) nor dissociated β-tryptase tetramers into monomers as shown by SEC and SDS-PAGE (Fig. 5a, b). The mutations at HC.S30 and HC.Y31 described above that improved the inhibitory potency of WT E82.AS were not sufficient to rescue the lost inhibitory effect in the context of the LC.D93G mutant (Fig. 4c). The lack of tetramer dissociation with this Fab was also observed by negative stain EM (Fig. 5c), where the tetramer with 4 Fabs is clearly evident.

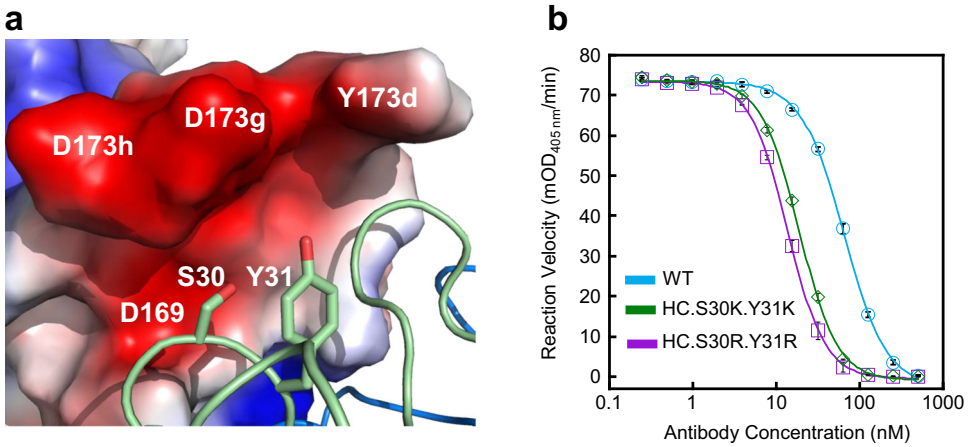

Fig. 3 | Mutation of E82.AS HC residues S30 and Y31 to Lys or Arg improves β-tryptase inhibition. a The structure of βI-tryptase bound to E82.AS is shown in surface and E82.AS heavy chain in cartoon (green). Negatively charged surface residues are shown in red (numbered) and positively charged surfaces are shown in blue. Mutated residues on E82.AS (light green) are shown in sticks. **b** Activity of 1 nM tetrameric βI-tryptase in the presence of E82.AS IgG variants at different concentration (2-fold dilution series). E82.AS mutants HC.S30K.Y31K (green) and HC.S30R.Y31R (purple) had IC_{50} values of 18.8 nM (3.4-fold) and 13.7 nM (4.7-fold), respectively; the fold improvement compared to WT E82.AS (blue), which had an IC_{50} of 64.2 nM, is in parenthesis. Data is represented as mean ± s.d. ($n = 3$ independent experiments). Source data are provided as a Source Data file.

We hypothesized that the conformational changes in the 220 s loop, instigated by the rearrangement of N223, were transduced to the active site via the disulfide bond between C191 and C220. This disulfide connects the 220 s to the 180 s loop and is displaced 5.2 Å at C191 and 2 Å at C220 in the E82.AS-bound structure (Fig. 4a) and thereby relays the structural rearrangement in the 220 s loop to the 180 s loop. To demonstrate this connection, we first stabilized the catalytically active conformation of the 180 s loop (oxyanion hole and N-terminal insertion) in WT tetrameric tryptase with the irreversible active site inhibitor Glu-Gly-Arg-chloromethylketone (EGR-cmk) covalently bound to S195 and then formed a complex with WT Fab E82.AS. SEC analysis showed a major peak in which four E82.AS Fabs were bound to active site-inhibited tetrameric tryptase with only a minor peak showing monomeric tryptase bound to E82.AS (Fig. 5a, b). This implies that the transduction of the structural changes in the 220 s loop can be stopped if the active conformation in the 180 s loop is stabilized and thus keeps the tetramer intact. Altogether, we conclude that E82.AS binding to tetrameric tryptase causes conformational changes in the 220 s loop solely by E82.AS LC residue D93, which are further transduced via the disulfide bond C191-C220 to the 180 s loop and subsequently to the active site. This leads to the release of I16 from the activation domain pocket, tetramer dissociation into monomers, and a transition to a zymogen-like conformation with no activity, even in the presence of high amounts of heparin.

Discussion

Mast cell activation in healthy and diseased states via IgE-mediated Fcε receptor crosslinking on the cell surface results in rapid secretion of a number of pro-inflammatory factors and proteases including tetrameric β-tryptase. Inflammatory diseases such as asthma, anaphylaxis and others, may be, in part, due to aberrant mast cell activation. Therefore, inhibitors of β-tryptases have broad therapeutic potential. We have previously described two anti-β-tryptase antibodies, 31A.v11 and E104.v2, which inhibit β-tryptase by dissociating the tetramer into monomers by either steric clashes of the Fabs when binding to the individual protomers in the tetramer (31A.v11, molecular pry bar)[10] or by simultaneous binding of two Fabs from one IgG (E104.v2) and steric strain on the tetramer exerted through the hinge region, which also leads to tetramer dissociation into monomers (E104.v2, molecular pliers)[50]. However, in both cases, residual enzymatic activity of antibody-bound monomers can be measured at high heparin concentrations, indicating that the active site cleft is still able to bind to substrates. Whether this amount of monomeric β-tryptase activity is physiologically relevant is unknown.

Here, we characterize an inhibitory anti-human β-tryptase antibody that results in tetramer dissociation via binding to an exosite that does not overlap with the 31A.v11 or E104.v2 binding epitope (Fig. 2a). In addition to dissociating the tetramer, E82.AS inhibits substrate binding to the active site of dissociated protomers, inhibiting any residual catalytic activity. Thus, E82.AS is a complete inhibitor of both tetrameric and monomeric β-tryptase, either as an IgG or a Fab, and is therefore superior in its MOA to 31A.v11 or E104.v2. To understand the MOA of E82.AS in greater molecular detail, we conducted biochemical and biophysical studies, enzymatic activity assays and determined a 3 Å cryoEM structure of E82.AS bound to monomeric tryptase. Consistent with slower exchange values in HDX-MS experiments, the binding epitope of E82.AS comprises the 160 s helix and some parts of 170 s and 220 s loops. This epitope is different from previously described anti-β-tryptase antibodies 31A.v11 and E104.v1 (Supplementary Fig. 9), which bind to residues in the 60 s, 80 s and 110 s regions of β-tryptase.

The structure revealed several key changes in the β-tryptase activation domain (N-terminus and 140 s, 180 s and 220 s loops) of β-tryptase that led to significant structural deformation of the catalytic site and substrate binding cleft (Fig. 6, Supplementary Fig. 10), such that the protease is inhibited and protein active site inhibitors like STI can no longer bind (Fig. 1a, b). We found that the allosteric inhibition stems from the 220 s loop shifting to accommodate D93 from the LC of E82.AS, which would otherwise result in a steric clash with N223 from tryptase (Fig. 4a). Replacement of Asp with Gly at residue 93 removed this steric clash and the antibody no longer inhibited β-tryptase (Fig. 4b), yet still bound to tryptase with subnanomolar binding affinity (Table 1) without dissociating tetramers into monomers (Fig. 5).

Furthermore, when we stabilized the active site conformation of tetrameric β-tryptase with a covalent active site inhibitor, WT E82.AS bound the inhibited tetramer, but no longer dissociated it to monomers as shown by SEC and SDS-PAGE (Fig. 5a, b, purple). This led us to conclude that only an unoccupied active site of tetrameric β-tryptase can transition to a zymogen-like conformation, where the N-terminal Ile16 is not inserted and the tetramer dissociates into monomers. E82.AS likely stabilizes this dissociated zymogen-like conformation of the protease and subsequently locks it into an inhibited state. This is

https://doi.org/10.1038/s41467-026-70491-3

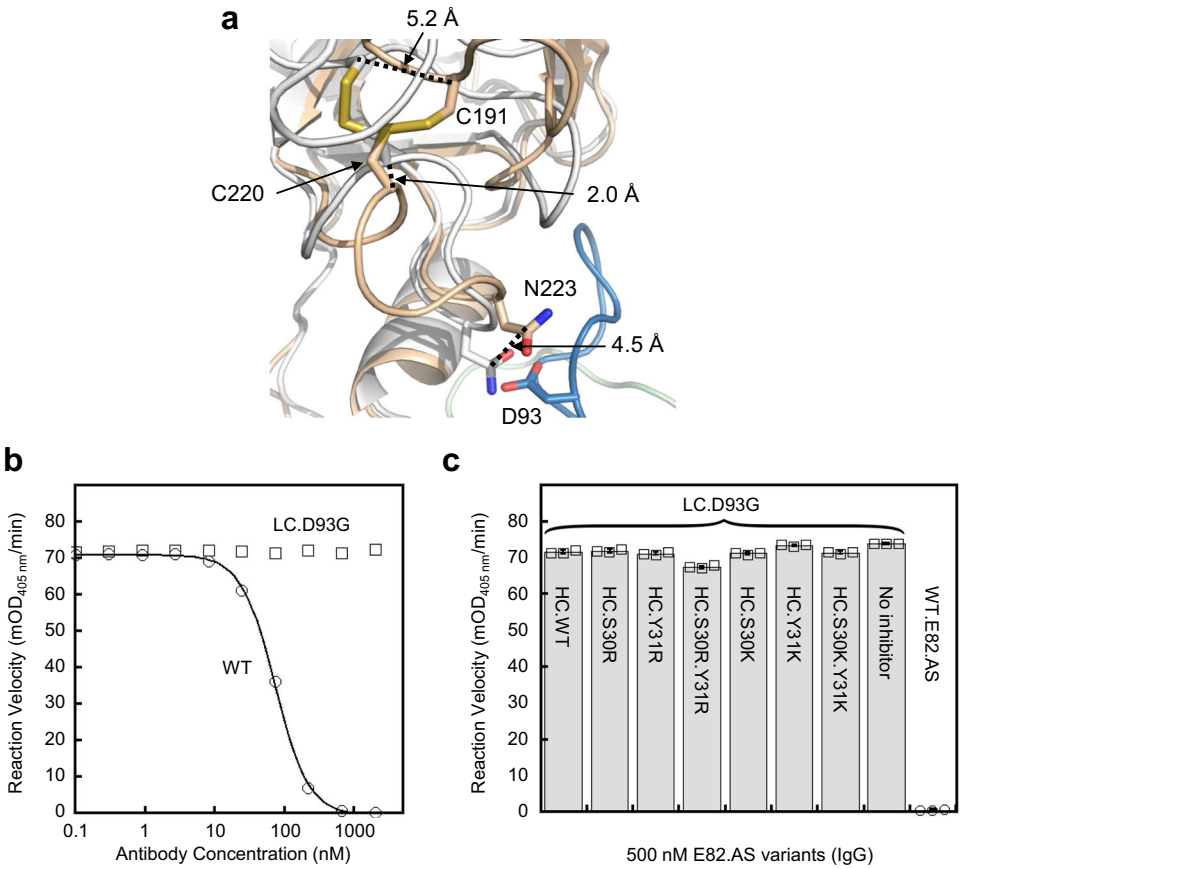

Fig. 4 | E82.AS light chain mutant D93G does not inhibit β-tryptase. a βI-Tryptase N223 shifts to accommodate D93 from the light chain of E82.AS. Light chain of E82.AS is in blue. WT βI-tryptase (gray) and βI-tryptase bound to E82.AS (beige) are structurally aligned and shown in cartoon. N223 moves by 4.5 Å from its wild-type conformation to avoid a steric clash with LC.D93 upon E82.AS binding. Disulfide bond C191-C220 is shown in sticks with a 5.2 Å and 2.0 Å shift for Cys191 and Cys220, respectively, between unbound and E82.AS bound β-tryptase. **b** Activity of 1 nM tetrameric βI-tryptase in the presence of E82.AS IgG WT (open circles) or LC.D93G mutant (open squares). Graph is a representative of multiple repeats. **c** Activity of 1 nM tetrameric βI-tryptase was carried out in the presence of 500 nM E82.AS IgG WT (open circles) or E82.AS IgG heavy chain variants in LC.D93G background (open squares). Data is represented as mean ± s.d. ($n = 3$ independent experiments). Source data are provided as a Source Data file.

consistent with our previous work, where we showed that tetramer formation cannot occur with an I16G variant, which, after pro-domain removal, can no longer insert its N-terminus into the activation domain pocket[19]. In general, N-terminal insertion into the activation domain pocket requires both a hydrophobic side chain interaction and a salt bridge with D194, and is a hallmark of trypsin-like serine protease activation transitioning from zymogen to enzyme conformation[54].

The 220 s loop and the 180 s loop are connected via the disulfide bond C191-C220. In a domino-like effect, this connection transduces the conformational changes from N223 to the 180 s loop and ultimately eliminates the oxyanion hole and I16 insertion (Fig. 6). A previous report has shown that the disulfide bond C191-C220 is redox active and can be stoichiometrically reduced by thioredoxin to reduce the enzymatic activity[55]. Mutations or elimination of the equivalent disulfide bond in other trypsin-like proteases (S1A superfamily) such as coagulation factor XII and thrombin results in reduction or complete of loss of activity[56,57]. Increasing potency of E82.AS, by introducing the double mutant HC.S30R.Y31R, did not rescue the loss of inhibitory activity created by the LC.D93G mutation, indicating that LC.D93 is the key driver of the allosteric inhibition (Fig. 4c). Altogether, this allows us to understand the entire molecular trajectory of the allosteric path leading to inhibition.

Additional structural heterogeneity that we have observed in the small and large tetramer interfaces in the E82.AS-bound structure are likely a consequence of β-tryptase being monomeric and not the cause for tetramer dissociation. Interestingly, and unlike antibody 31A.v11[10], we noticed that E82.AS binding, when modeled on tetrameric tryptase, does not result in steric clashes amongst the 4 individual Fabs or with a neighboring tryptase protomer (Supplementary Fig. 11).

There are a number of antibodies described that show specific inhibition of serine proteases with different modes of inhibition such as blocking the orthosteric site or allosteric inhibition via binding to an exosite, also known as the "allosteric switch" mechanism[49]. Allosteric exosites of such inhibitory antibodies of trypsin-fold serine proteases have been located in the 99 s loop on HGFA (Fab40) (PDB: 3K2U)[58], the 140 s loop on FXI (Fab BAY1213790) (PDB: 6HHC)[59] and uPA (mAb-112) (PDB: 4DW2)[60], and the 170 s loop on Factor D (PDB:4D9Q)[61], hepsin (Fab hH35) (PDB: 3T2N)[62], and hKLK5 (PDB: 7U5B)[63]. Except for the Factor D Fab (AFD), binding leads to conformational changes in the active site cleft rendering the enzyme catalytically incompetent, but the allosteric path has not been clearly described for these complexes. The structures of uPA, hepsin and hKLK5 bound to their inhibitory Fabs also show the absence of the oxyanion hole, loss of N-terminal insertion and conformational heterogeneity in the 180 s and 220 s loops. Disruption of the oxyanion hole is not found in the AFD-Factor D structure. This is not unexpected since AFD binding does not disrupt enzymatic activity, but instead blocks interaction with C3b and downstream complement activation. Similar to E82.AS, the hepsin antibody hH35 shows binding to the 170 s and 220 s loops, however, the binding angle and interactions differ. The 220 s loop in hepsin

https://doi.org/10.1038/s41467-026-70491-3

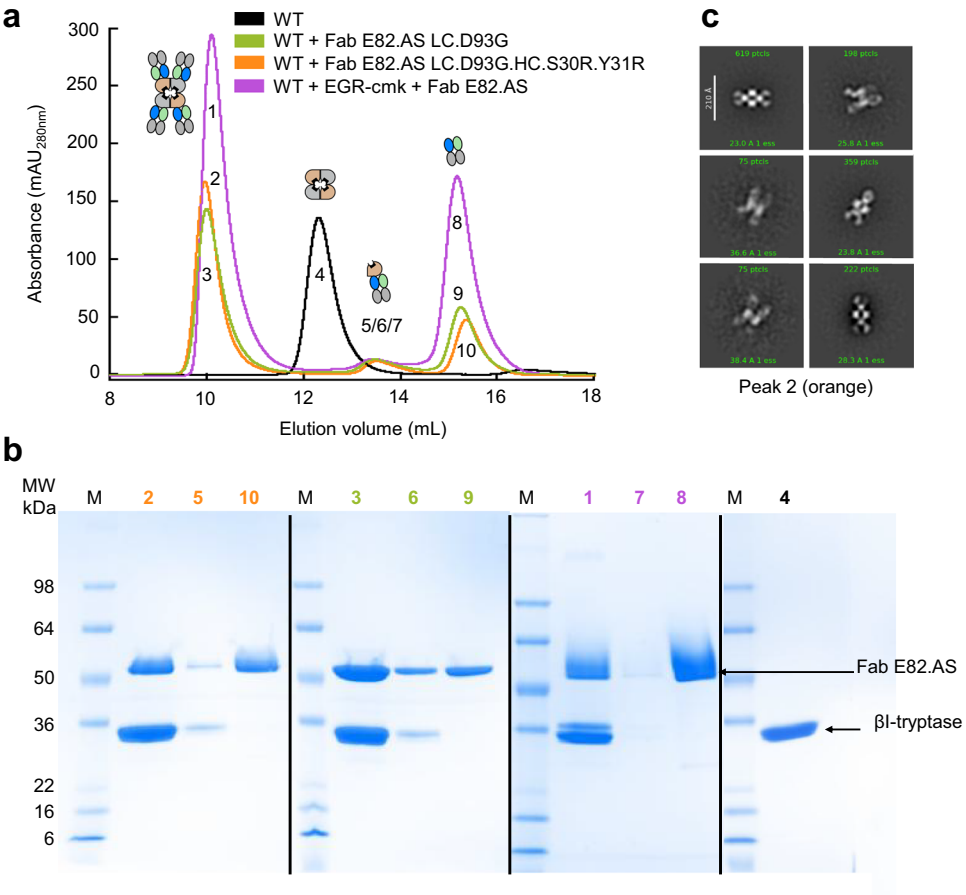

Fig. 5 | E82.AS Fab mutants binding to WT β-tryptase in the presence and absence of a covalent active site inhibitor. a Size exclusion chromatography of tetrameric tryptase alone (black) and with 2-fold molar excess of Fab LC.D93G mutant (green), LC.D93G.HC.S30R.Y31R mutant (orange) are shown. Fab E82.AS with βI-tryptase covalently bound with the active site inhibitor Glu-Gly-Arg-chloromethylketone (EGR-cmk) is in purple. Tetrameric tryptase with Fab WT E82.AS is shown in blue in Fig. 1b. **b** Fractions of the peaks were analyzed by SDS-PAGE in 4 individual gels. The peak numbers are color-coded according to Fig. 5a; M refers to MW markers. **c** Peak 2 (orange) with E82.AS LC.D93G.HC.S30R.Y31R was analyzed in negative stain EM showing tetrameric species with four E82.AS mutant Fabs bound. These are representative class averages from 4086 particles classified into 50 classes. The data shown in panels **a** and **b** is representative of 3 independent experiments. Source data are provided as a Source Data file.

adopted a new conformation to avoid clashing with hH35. In addition, significant parts of the 180 s and 220 s loops cannot be resolved in the crystal structure, indicating heterogeneity in these regions. The authors suggested that this leads to conformational changes in the oxyanion hole as well the catalytic triad residues, which explains the inhibition. Thus, allosteric inhibition of trypsin-like serine proteases can be achieved by structural alteration of the N-terminus and the 180 s and 220 s loops that lead to destruction of a competent active site, but the binding epitope and the orientation of the bound inhibitor can differ from case to case.

CryoEM determines structures free from the constraints and contacts of a crystal lattice and have the advantage of allowing structural heterogeneity and revealing flexibility within a protein. This gave us the opportunity to determine which regions within β-tryptase show increased flexibility when bound to the inhibitory antibody E82.AS with an unoccupied active site, such as the unresolved N-terminus and the 140 s loop, while still allowing us to visualize high-resolution information at the binding epitope and alternate conformations in the active site and 180 s loop. Furthermore, the mutant E82.AS LC.D93G is a rare example of an antibody in which binding and activity can be almost completely decoupled via a single mutation. To our knowledge, there are only two published examples where a single mutation in the framework residues of an antibody had minimal to no effect on binding affinity, but had a strong effect on activity. In one case, mutation of the framework residue V11L in the humanized anti-CD20 antibody GA101 causes a loss in activity, but retains binding[64]. In another case, framework residue variations at either position 19, 79 or 81 (Kabat numbering) in the HC of anti-TGFβ−2/3 antibody h4A11 can cause gain or loss of inhibitory activity without affecting binding affinity[65].

While E82.AS is a potent inhibitor of human β-tryptase, it still contains rabbit variable domain sequences. Prior to testing this antibody in the clinic, full humanization would be required for developing it as a therapeutic to avoid any unwanted immunogenicity. This process would involve grafting the CDRs in a human germline as we have previously described[50].

Any inhibition of tryptase in a clinical setting must be taken with great care. While excess tryptase may lead to adverse physiological effects[2,4,6], tryptase also has important vital roles as well. Mast cell tryptase cleaves a very restricted number of human cytokines (TSLP, IL-21) and chemokines (MCP3, MIP-3b, and eotaxin), implying an important immune regulatory role in controlling excessive TH2-mediated inflammation[66]. Prolonged inhibition might lead to a diminished allergic response as well as excessive levels of TH2 cytokines. Thus, the extent to which tryptase inhibition may have clinical benefit must be balanced with its inherent positive functions.

Our work provides detailed insights into the trajectory and the MOA of the allosteric inhibition of tetrameric tryptase by E82.AS. Such

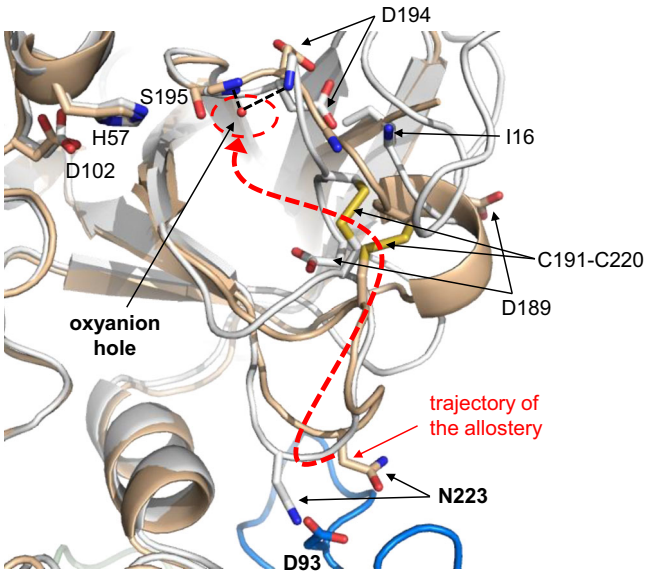

Fig. 6 | Trajectory of the allosteric inhibition of β-tryptase. A protomer from WT tetramer βI-tryptase (PDB: 1A0L) in gray and E82.AS-bound βI-tryptase in beige are structurally aligned. The proposed trajectory of the allostery starting at N223 resulting from a steric clash by D93 from the light chain of E82.AS (blue) to the active site is traced with a dashed red arrow. Key residues involved along the allosteric path are labeled. The oxyanion hole is shown as a small red sphere in a dashed red oval with dashed lines to main chain nitrogen atoms of G193 and S195. Catalytic triad residues H57, D102 and S195 are shown in sticks.

allosteric, inhibitory antibodies of multimeric serine proteases are rare to find. Another such inhibitory antibody is anti-HtrA, which completely rearranges the active site while binding to a loop 30 Å away[67]. Since E82.AS can completely inhibit both tetrameric and monomeric human β-tryptase as a Fab in the presence of heparin, it may have increased value for therapeutic intervention in β-tryptase-dependent mast cell related diseases.

Methods

Recombinant expression of WT and β-tryptase mutants

The sequence encoding mature wild-type (WT) human βI-tryptase (Uniprot Q15661) from I31 - P275 (I16 - P246 chymotrypsinogen numbering[52]) was cloned into a modified pAcGP67A vector behind the polyhedron promoter and the gp67 secretion signal sequence. Expression constructs contain an N-terminal His_6-tag, followed by an enterokinase (EK) cleavage site directly fused to the mature N-terminal I16 of β-tryptase. Site-directed mutagenesis was performed using standard QuikChange protocols (Agilent, Santa Clara CA) to generate β-tryptase mutants. All constructs were confirmed by DNA sequencing. Recombinant baculovirus were generated using the Baculogold system (BD Biosciences, San Jose CA) in Sf9 insect cells (Expression Systems, Davis CA) following standard protocols. Tni insect cells (Expression Systems, Davis CA) were infected for large-scale protein production and harvested 48 h post-infection. The harvested media was supplemented with 1 mM $NiCl_2$, 5 mM $CaCl_2$ and 20 mM Tris pH 8, shaken for 30 min and then centrifuged for 20 min at 8500 x g to remove the cells and precipitate from media. The supernatant media was filtered through a 0.22 μm PES filter prior to loading onto a Ni-NTA affinity column.

Insect cell media containing secreted His_6-tagged zymogen βI-tryptase (WT or mutant) was loaded onto a 10 mL Ni-NTA Superflow column (Qiagen, Germantown, MD) at a volumetric flow rate of 170 cm/h. The column was washed with 10 column volumes (CV) of wash buffer (20 mM Tris pH 8, 10 mM imidazole, 300 mM NaCl) and eluted with 8 CV elution buffer (20 mM Tris pH 8, 300 mM imidazole, 300 mM NaCl). Fractions assayed by SDS-PAGE containing βI-tryptase were pooled, concentrated and loaded onto an S200 column (GE Healthcare, Piscataway, NJ) for further purification by size-exclusion chromatography (SEC) using SEC buffer (10 mM MOPS pH 6.8, 2 M NaCl) at flow rates recommended by manufacturer. Fractions containing zymogen βI-tryptase monomer were pooled and concentrated. Zymogen βI-tryptase was then cleaved overnight at room temperature at a concentration of 2 mg/mL in 10 mM MOPS pH 6.8, 0.2 M NaCl containing 0.5 mg/mL heparin (H3393; average MW ~ 18 kDa; Sigma Aldrich, St. Louis, MO) and 0.1 mg/mL EK (NEB, Ipswich, MA). This step removes the N-terminal His_6-tag and results in tetramerization and proteolytically active βI-tryptase, which has IVGG as the newly formed N-terminal sequence starting at residue 16. Tetrameric βI-tryptase was then subjected to SEC using an S200 column (GE Healthcare, Piscataway, NJ) in SEC buffer to purify tetrameric βI-tryptase by removing EK and any uncleaved zymogen βI-tryptase. βI-Tryptase mutants Y75C and I99C were purified by Ni-affinity chromatography as described above. Disulfide-linked βI-tryptase dimer mutants were then separated from non-disulfide linked βI-tryptase monomer mutants by SEC on an S200 column as above. Disulfide-linked dimer mutants were further processed by EK cleavage as described above for WT βI-tryptase to form active tetramers (mutants Y75C and I99C).

Generation and purification of anti-β-tryptase antibodies and the anti-kappa nanobody

Human chimeric anti-β-tryptase variants (rabbit variable light (VL) and variable heavy (VH)) were expressed by transient transfection of CHO K1 cells (WuXi Biologics). Antibodies were purified by affinity chromatography and SEC using standard methods (MabSelect SuRe; GE Healthcare, Piscataway, NJ). E82.AS is a human chimeric IgG1 antibody with the variable light (VL)-constant light (CL) rabbit disulfide changed to C80A and C171S. The anti-kappa nanobody[53] was produced in HEK293 cells (ChemPartners) by transient transfection and purified using standard Ni-affinity chromatography followed by size exclusion chromatography using an S-75 column in 20 mM histidine acetate pH 5.5, 150 mM NaCl buffer.

Production of chimeric Fab E82.AS

Chimeric Fabs of the antibodies were prepared by incubating the antibody with lysyl endopeptidase (Wako Chemicals, Inc.) at 37 °C for 1 h at an enzyme to antibody ratio of 1:500. After 1 h, the reaction was quenched by adding 1/10 volume of 10% acetic acid and the Fab and Fc fragments were separated by cation exchange chromatography (50 mM Na-acetate buffer pH 5, NaCl gradient 0-1 M over 20 column volumes) using a 5 mL HiTrap SP HP column (GE Healthcare, Piscataway, NJ). The isolated Fabs were subjected to a final purification step on an S-200 SEC column (GE Healthcare, Piscataway, NJ) in PBS.

β-Tryptase enzymatic activity assay

The enzymatic activity of 1 nM tetrameric βI-tryptase was measured in 200 μL volume using 2 mM S-2288 chromogenic substrate (DiaPharma Group, Inc., West Chester, OH) was performed as previously described[19] using TN (20 mM Tris pH 8.0, 150 mM NaCl), TNH1 (20 mM Tris pH 8.0, 150 mM NaCl, 1 μg/mL heparin) or TNH100 (20 mM Tris pH 8.0, 150 mM NaCl, 100 μg/mL heparin) buffers as indicated. The reaction velocity was determined by the rate at which p-nitroaniline (pNA) is released, which was measured spectrophotometrically at 405 nm using a SpectraMax M5e plate reader using Softmax Pro (v6.2.2) (Molecular Devices, Sunnyvale, CA). Inhibition plots were generated using 4-parameter fits from data collected from 3 independent experiments and statistical analysis was performed using KaleidaGraph (v5.0.6) (Synergy Software, Reading, PA).

Complex formation of βI-tryptase tetramers with Fabs

Tetrameric βI-tryptase, wild-type or mutants Y75C or I99C, were mixed with a 2-fold molar excess of Fab and incubated for 15 min at 25 °C. The

mixture was then subjected to S200GL size exclusion column (25 mL bed volume, GE Healthcare, Piscataway, NJ) chromatography in either tryptase SEC buffer (10 mM MOPS pH 6.8, 2 M NaCl) or TNH100 (20 mM Tris pH 8.0, 150 mM NaCl, 0.1 mg/mL Heparin) buffer. All fractions containing protein as indicated by absorbance at $A_{280\ nm}$ were analyzed by SDS-PAGE under non-reducing conditions to identify the protein components in these fractions. SeeBlue™ Plus2 pre-stained protein standard (ThermoFisher, Waltham, M A) was used for molecular weight markers for SDS-PAGE analysis.

Hydrogen deuterium exchange mass spectrometry analysis

Deuterium uptake rates of zymogen βI-tryptase monomer in the presence and absence of antibody E82.AS was measured to determine structural regions that are modified upon antibody binding. Bound samples contained 1:1 mixture of zymogen βI-tryptase and the respective antibody (98% bound using measured dissociation constants) prepared and incubated at 25 °C for 1 h. Zymogen βI-tryptase concentration prior to deuterium labeling was 30 µM in Ab bound and unbound samples. HDX-MS experiments consisted of diluting samples 20-fold into deuterium labeling buffer containing 20 mM histidine acetate at pD 7.0 (Serva Electrophoresis GmbH, Heidelberg, Germany) at 5 °C. Six labeling times (0.5, 2, 10, 54, 278, and 1440 min) were sampled in triplicate, quenched by lowering the pH to 2.5 and the addition of 2 M guanidinium chloride (Sigma Aldrich, St. Louis, MO) and 0.25 M TCEP (Sigma Aldrich, St. Louis, MO) using an extended, parallel arm LEAP HDX automation system (Trajan Scientific, Chronos software Version 5. 1. 10). Samples were first passed through an immobilized 50:50 Fungal protease/Pepsin column (NovaBioAssays) and loaded onto an online trap column (Acquity Vanguard C8, Waters) for desalting at 150 µL/min for 2 min at 0 °C. Peptide fragments were then separated by reversed-phased chromatography (35 µL/min) where they were introduced into the mass spectrometer by electrospray ionization (Thermo Q-Exactive, 120 kHz resolution at m/z 400) for mass analysis. To further minimize back-exchange, 0.04% v/v TFA was added to mobile phases containing 0.1% formic acid to adjust their pH approximately to 2.25. The levels of recovery on average are thus expected to be roughly 85%[68].

Protein Metrics Byonic (Version 4.5.2) and Byologic (Version 4.5-53 ×64) software was used for peptide identification (FDR2D filter of ≤ 0.0001) followed by ExMS 2.0[69] (Version 03NOV2018) to provide XIC's and deuterium uptake levels for each peptide across the sampled timepoints using recommended settings was used to identify deuterated peptides and prepare extracted ion chromatograms, which were then analyzed for deuterium content using in-house implementations of a n-population binomial analysis using a statistical *F*-test[70]. Prior to fitting isotopic distributions, degenerate charge states were combined by direct summation of equivalent peak intensities.

A total of 195 peptides (Supplementary Fig. 12) covering 88.8% of tryptase with an average redundancy of 10.60 unique peptides per residue were included for PF analysis using the empirical method[71], with errors defined by the SEM of triplicate measurements. The value observed for the smallest peptide for each residue was taken as the change in protection, or ΔPF, for that residue. A spreadsheet, available in Supplementary Data 1 contains a coverage map, standard summary statistics[72], βI-tryptase sequence in full length and chymotrypsinogen numbering, the empirical PF value along with the error in its measurement for all peptides used to define the PF plot, annotations for residues contacting the antibody E82.AS as well as those involved in allosteric changes that lead to inactivation of βI-tryptase upon binding.

To determine significance of the measured PF, we used our previously published combinatorial approach to estimate error[50]. This estimation gives an asymmetric error about the mean, thus the term positive and negative below. A value was considered significant if its magnitude exceeded the SEM. For protected regions (log(PF) > 0), the value had to be larger than the negative error. For deprotected regions (log(PF) < 0), the absolute value had to be greater than the positive error. Nonsignificant values are reported as zero in the Smallest Peptide tab of Supplementary Data 1. In regions where the PF was obviously much larger than could be estimated by this empirical method, the peptide was flagged as stated in the Notes column. Finally, the sequence and numbering of the protein used for HX experiments as well as chymotrypsinogen numbering[52] is included for any necessary disambiguation as a tab in this spreadsheet.

Cryogenic electron microscopy data collection and image processing

The E82.AS:βI-tryptase:E104.v2:Nb complex was formed by incubating all components at a 1:1:1:1 ratio for 1 hour before running through an S200 gel filtration column in 20 mM HEPES pH 7.5, 100 mM NaCl buffer. The peak fraction was diluted to 0.25-0.3 mg/mL in 20 mM HEPES pH 7.5, 100 mM NaCl directly before vitrification, and 2.5 µL sample was applied to glow-discharged holey gold 0.6/1 300-mesh grids (Quantifoil). Grids were blotted for 3 s at 7 force before being plunge vitrified in liquid ethane using a MarkIV Vitrobot (ThermoFisher). The blotting chamber was maintained at 4 °C and 100% humidity during freezing.

Movies were collected using a Titan Krios G3i (ThermoFisher) outfitted with a K3 camera and Bioquantum energy filter (Gatan). The K3 detector was operated in nonCDS counting mode and the energy filter slit width was set to 20 eV. Movies were collected at a nominal magnification of 105,000×, physical pixel size 0.838 Å $pixel^{-1}$, with a 50 µm C2 aperture and 100 µm objective aperture at a dose rate of 15 e^- $pixel^{-1}$ s^{-1}. A total dose of 64 e^- $Å^{-2}$ was collected as a 59-frame movie, resulting in a 3 s movie with 1.08 e^- per frame. Data were collected using semi-automated imaging scripts in SerialEM (v4.1.25)[73]. 4,710 movies were collected in a 3 × 3 image shift pattern at 0° tilt, 2739 at 15°, 3210 at 30°, and 2442 at 40° in consecutive data collections. Beam tilt was corrected for using SerialEM's image shift vs coma calibration. Raw cryo-EM movies have been deposited in EMPIAR[74] as EMPIAR-13094.

Data were processed on-the-fly through 2D classification using cryoSPARC (v4.2.1 and v5.1.0)[75]. Movies were motion corrected using patch motion correction, CTF information was estimated using patch CTF estimation, and micrographs were curated based off of CTF resolution fit. Templates created from a ~ 9 Å map from data collected on a Glacios (ThermoFisher) outfitted with a K2 camera (Gatan) were used for particle picking. Template picking yielded 8,899,017 picks, roughly evenly split across the collections. These were extracted in a 420-pixel box, and binned to 128 pixels. 2D classification was run with default settings and a circular mask of 140 Å. 'Good' (showing at least one Fab) class averages were selected and 6,338,581 particles were moved into 3D sorting. Four ab initio classes were generated from the 0° tilt data, 2,262,677 particles, one showing density for a single Fab, one resembling an amorphous blob, one showing the expected complex of tryptase and two Fabs, and one showing roughly two copies of tryptase with two Fabs. All particles were subjected to four rounds of heterogeneous refinement using these volumes as starting models, with two copies of the 'correct' complex. 1,160,676 particles were re-extracted in a 450-pixel box, and binned to 256 pixels. One round of heterogeneous refinement was run with no downsampling. 716,327 particles were re-extracted in a 450-pixel box, and binned to 324 pixels, giving a final pixel size of 1.164 Å $pixel^{-1}$. One round of heterogeneous refinement was run, particles downsampled to 256 pixels. Two classes, constituting 680,181 particles, were subjected to non-uniform refinement. Both classes clearly showed the intact complex, with one centered on Fab E82.AS and one centered on tryptase. The classes with tryptase centered was used as an initial model and filtered to 15 Å before refinement. Non-uniform refinement was run after reference-based motion correction, per-particle defocus, per-group CTF parameter optimization, and duplicates were removed. The final map from

672,348 particles was estimated to be 3 Å by gold-standard FSC. Local resolution, orientation diagnostics and local filtering jobs were run on the final map.

For β-tryptase and E104.v2, a previous crystal structure (PDB: 6VVU) was used as an initial model. An Alphafold2 model of Fab E82.AS was used as an initial model. The nanobody was rigid fit into the density from the crystal structure PDB: 6ANA. Because of the low resolution of the map in this region, side chains were not assigned. The initial templates were rigid fit into the cryoEM map of E82.AS:βI-tryptase:E104.v2:Nb using ChimeraX (v1.7.1)[76]. The models were manually fit and mutated in E82.AS and E104.v2 with ISOLDE (v1.6)[77]. The model was refined in Phenix real space refinement[78]. Model geometry and map-to-model statistics were assessed using the EM validation check in Phenix (v1.20.1-4487). CryoEM data collection, refinement and validation statistics are presented in Supplementary Table 1. Figures were prepared in ChimeraX and PyMol (version 3.1.3)[79].

To create a complete structure to enable a morph between the enzyme and zymogen conformations, otherwise disordered loop residues (residues 16-25 and residues 141-155) were grafted into our E82.AS/E104.v2-bound structure PDB:9MNB from a β-tryptase protomer of 1A0L. The peptide geometry of the fusion points was improved using Coot's Bond regularization tools. The overall positions of these two loops were then manually adjusted outwards using the 'sculpting' function of PyMOL to create a potential zymogen-like conformational model for these specific areas while maintaining reasonable backbone geometry. Supplementary Movie 1 was made in ChimeraX using the morph function between the active enzyme conformation of β-tryptase as seen in the tetrameric state (PDB:1A0L) and this computationally-derived fusion that represents the E82.AS/E104.v2-bound β-tryptase structure in its inhibited zymogen-like structure.

Epitope binning and competition binding of antibodies E82.AS, 31A.v11 and E104.v2

The epitope binning assay, a label free dip and read assay, was run using Octet RED384 system (Sartorius Corporation, USA). The assay buffer was Phosphate-Buffered Saline (PBS) containing 0.5% Bovine Serum Albumin and 0.05% Polysorbate 20. Briefly biotinylated human β-tryptase, diluted at 10 µg/mL in assay buffer, was captured using streptavidin Octet biosensor tip (cat # 18-5019, Sartorius Corporation, USA) for 200 s followed by binding of the first mAb, E82.AS hIgG1 at 20 µg/mL for 600 seconds to saturation. The cross-blocking was observed by dipping the saturated sensor into the second mAb at 5 µg/mL for 300 s. An increase in signal upon dipping into the second mAb indicates that both antibodies can bind simultaneously to β-tryptase and bind distinct epitopes.

Affinity and binding kinetics measurements of E82.AS variants by surface plasmon resonance

Antibody binding affinity was determined using a capture assay using the Biacore T200 system from Cytiva, USA. Briefly anti-human capture antibody was covalently immobilized onto a CM5 chip. Subsequently, the ligand, anti-β-tryptase antibodies with a human backbone, were captured on the chip for 20 s. This was followed by passing different concentrations of the analyte, zymogen βI-tryptase monomer, over the chip. The resulting binding kinetic data was then collected and analyzed using Cytiva evaluation software, employing a 1:1 binding model.

Reporting summary

Further information on research design is available in the Nature Portfolio Reporting Summary linked to this article.

Data availability

The 3D-EM map generated in this study has been deposited into the Electron Microscopy Data Bank under accession code EMD-48419 and the coordinates of the complex have been deposited in the PDB with accession code 9MNB. These will be publicly available as of the date of publication. HDX-MS data for E82.AS binding to zymogen βI-tryptase monomer have been deposited in the MassIVE Repository with accession code MSV000098179 [https://massive.ucsd.edu/ProteoSAFe/dataset.jsp?task=5873831b45534e7baa14d3becbf76ff0]. Raw cryo-EM movies have been deposited as EMPIAR-13094. The source data underlying Figs. 1a, c, d, 3b, 4b, c, 5b and Supplementary Fig. 2 are provided as a Source Data file. Published structures from the PDB referred to in this paper include 3K2U, 6HHC, 4DW2, 4D9Q, 3T2N, 7U5B, 6VVU, 6ANA and 1A0L. Source Data are provided as a Source Data file. Source data are provided with this paper.

References

1. Wernersson, S. & Pejler, G. Mast cell secretory granules: armed for battle. *Nat. Rev. Immunol.* **14**, 478–494 (2014).
2. Siebenhaar, F., Redegeld, F. A., Bischoff, S. C., Gibbs, B. F. & Maurer, M. Mast cells as drivers of disease and therapeutic targets. *Trends Immunol.* **39**, 151–162 (2018).
3. Frossi, B., Mion, F., Tripodo, C., Colombo, M. P. & Pucillo, C. E. Rheostatic functions of mast cells in the control of innate and adaptive immune responses. *Trends Immunol.* **38**, 648–656 (2017).
4. Caughey, G. H. Mast cell proteases as pharmacological targets. *Eur. J. Pharm.* **778**, 44–55 (2016).
5. Pejler, G., Abrink, M., Ringvall, M. & Wernersson, S. Mast cell proteases. *Adv. Immunol.* **95**, 167–255 (2007).
6. Pejler, G. The emerging role of mast cell proteases in asthma. *Eur. Respir. J.* **54**, 1900685 (2019).
7. Berger, P. et al. Tryptase and agonists of PAR-2 induce the proliferation of human airway smooth muscle cells. *J. Appl Physiol.* **91**, 1372–1379 (2001).
8. Cairns, J. A. & Walls, A. F. Mast cell tryptase stimulates the synthesis of type I collagen in human lung fibroblasts. *J. Clin. Invest* **99**, 1313–1321 (1997).
9. Woodman, L. et al. Mast cells promote airway smooth muscle cell differentiation via autocrine up-regulation of TGF-β1. *J. Immunol.* **181**, 5001–5007 (2008).
10. Maun, H. R. et al. An allosteric anti-tryptase antibody for the treatment of mast cell-mediated severe asthma. *Cell* **179**, 417–431.e419 (2019).
11. Cairns, J. A. Inhibitors of mast cell tryptase beta as therapeutics for the treatment of asthma and inflammatory disorders. *Pulm. Pharm. Ther.* **18**, 55–66 (2005).
12. Rawlings, N. D. et al. The MEROPS database of proteolytic enzymes, their substrates and inhibitors in 2017 and a comparison with peptidases in the PANTHER database. *Nucleic Acids Res.* **46**, D624–D632 (2017).
13. Le, Q. T. et al. Processing of human protryptase in mast cells involves cathepsins L, B, and C. *J. Immunol.* **187**, 1912–1918 (2011).
14. Schwartz, L. B. & Bradford, T. R. Regulation of tryptase from human lung mast cells by heparin. Stabilization of the active tetramer. *J. Biol. Chem.* **261**, 7372–7379 (1986).
15. Addington, A. K. & Johnson, D. A. Inactivation of human lung tryptase: Evidence for a re-activatable tetrameric intermediate and active monomers. *Biochemistry* **35**, 13511–13518 (1996).
16. Ren, S., Sakai, K. & Schwartz, L. B. Regulation of human mast cell β-tryptase: Conversion of inactive monomer to active tetramer at acid pH. *J. Immunol.* **160**, 4561–4569 (1998).
17. Schechter, N. M., Choi, E. J., Selwood, T. & McCaslin, D. R. Characterization of three distinct catalytic forms of human tryptase-β: their interrelationships and relevance. *Biochemistry* **46**, 9615–9629 (2007).
18. Hallgren, J., Lindahl, S. & Pejler, G. Structural requirements and mechanism for heparin-dependent activation and tetramerization of human βI- and βII-tryptase. *J. Mol. Biol.* **345**, 129–139 (2005).

19. Maun, H. R. et al. Dual functionality of β-tryptase protomers as both proteases and cofactors in the active tetramer. *J. Biol. Chem.* **293**, 9614–9628 (2018).
20. Fajardo, I. & Pejler, G. Formation of active monomers from tetrameric human β-tryptase. *Biochem J.* **369**, 603–610 (2003).
21. Fukuoka, Y. & Schwartz, L. B. Human β-tryptase: detection and characterization of the active monomer and prevention of tetramer reconstitution by protease inhibitors. *Biochemistry* **43**, 10757–10764 (2004).
22. Fukuoka, Y. & Schwartz, L. B. Active monomers of human β-tryptase have expanded substrate specificities. *Int. Immunopharmacol.* **7**, 1900–1908 (2007).
23. Franconi, G. M., Graf, P. D., Lazarus, S. C., Nadel, J. A. & Caughey, G. H. Mast cell tryptase and chymase reverse airway smooth muscle relaxation induced by vasoactive intestinal peptide in the ferret. *J. Pharm. Exp. Ther.* **248**, 947–951 (1989).
24. Gruber, B. L. et al. Synovial procollagenase activation by human mast cell tryptase dependence upon matrix metalloproteinase 3 activation. *J. Clin. Invest* **84**, 1657–1662 (1989).
25. Maier, M., Spragg, J. & Schwartz, L. B. Inactivation of human high molecular weight kininogen by human mast cell tryptase. *J. Immunol.* **130**, 2352–2356 (1983).
26. Schiemann, F. et al. The cathelicidin LL-37 activates human mast cells and is degraded by mast cell tryptase: counter-regulation by CXCL4. *J. Immunol.* **183**, 2223–2231 (2009).
27. Schwartz, L. B., Bradford, T. R., Littman, B. H. & Wintroub, B. U. The fibrinogenolytic activity of purified tryptase from human lung mast cells. *J. Immunol.* **135**, 2762–2767 (1985).
28. Pereira, P. J. et al. Human β-tryptase is a ring-like tetramer with active sites facing a central pore. *Nature* **392**, 306–311 (1998).
29. Sommerhoff, C. P. et al. The structure of the human βII-tryptase tetramer: Fo(u)r better or worse. *Proc. Natl. Acad. Sci. USA* **96**, 10984–10991 (1999).
30. Hallgren, J., Backstrom, S., Estrada, S., Thuveson, M. & Pejler, G. Histidines are critical for heparin-dependent activation of mast cell tryptase. *J. Immunol.* **173**, 1868–1875 (2004).
31. Fukuoka, Y. & Schwartz, L. B. The B12 anti-tryptase monoclonal antibody disrupts the tetrameric structure of heparin-stabilized β-tryptase to form monomers that are inactive at neutral pH and active at acidic pH. *J. Immunol.* **176**, 3165–3172 (2006).
32. Alter, S. C., Kramps, J. A., Janoff, A. & Schwartz, L. B. Interactions of human mast cell tryptase with biological protease inhibitors. *Arch. Biochem Biophys.* **276**, 26–31 (1990).
33. Paesen, G. C. et al. A tick protein with a modified Kunitz fold inhibits human tryptase. *J. Mol. Biol.* **368**, 1172–1186 (2007).
34. Sommerhoff, C. P. et al. A Kazal-type inhibitor of human mast cell tryptase: Isolation from the medical leech *Hirudo medicinalis*, characterization, and sequence analysis. *Biol. Chem. Hoppe Seyler* **375**, 685–694 (1994).
35. Stubbs, M. T. et al. The three-dimensional structure of recombinant leech-derived tryptase inhibitor in complex with trypsin. Implications for the structure of human mast cell tryptase and its inhibition. *J. Biol. Chem.* **272**, 19931–19937 (1997).
36. Rothemund, S., Sonnichsen, F. D. & Polte, T. Therapeutic potential of the peptide leucine arginine as a new nonplant Bowman-Birk-like serine protease inhibitor. *J. Med Chem.* **56**, 6732–6744 (2013).
37. Murakami, Y. et al. Cyclotheonamide E4 and E5, new potent tryptase inhibitors from an *Ircinia* species of sponge. *J. Nat. Prod.* **65**, 259–261 (2002).
38. Avrutina, O. et al. Head-to-tail cyclized cystine-knot peptides by a combined recombinant and chemical route of synthesis. *Chembiochem* **9**, 33–37 (2008).
39. Sommerhoff, C. P. et al. Engineered cystine knot miniproteins as potent inhibitors of human mast cell tryptase β. *J. Mol. Biol.* **395**, 167–175 (2010).
40. Thongyoo, P., Bonomelli, C., Leatherbarrow, R. J. & Tate, E. W. Potent inhibitors of beta-tryptase and human leukocyte elastase based on the MCoTI-II scaffold. *J. Med Chem.* **52**, 6197–6200 (2009).
41. Scarpi, D., McBride, J. D. & Leatherbarrow, R. J. Inhibition of human beta-tryptase by Bowman-Birk inhibitor derived peptides: creation of a new tri-functional inhibitor. *Bioorg. Med Chem.* **12**, 6045–6052 (2004).
42. McGrath, M. E. et al. Structure-guided design of peptide-based tryptase inhibitors. *Biochemistry* **45**, 5964–5973 (2006).
43. Ni, W. W., Cao, M. D., Huang, W., Meng, L. & Wei, J. F. Tryptase inhibitors: a patent review. *Expert Opin. Ther. Pat.* **27**, 919–928 (2017).
44. Qian, X., Zheng, B., Burke, B., Saindane, M. T. & Kronenthal, D. R. A stereoselective synthesis of BMS-262084, an azetidinone-based tryptase inhibitor. *J. Org. Chem.* **67**, 3595–3600 (2002).
45. Sutton, J. C. et al. Synthesis and SAR of 4-carboxy-2-azetidinone mechanism-based tryptase inhibitors. *Bioorg. Med Chem. Lett.* **12**, 3229–3233 (2002).
46. Wright, C. D. et al. Inhibition of allergen-induced pulmonary responses by the selective tryptase inhibitor 1,5-bis-[4-[(3-carbamimidoyl-benzenesulfonylamino)-methyl]-phenoxy]-pen tane (AMG-126737). *Biochem Pharm.* **58**, 1989–1996 (1999).
47. Costanzo, M. J. et al. Potent, nonpeptide inhibitors of human mast cell tryptase. Synthesis and biological evaluation of new spirocyclic piperidine amide derivatives. *Bioorg. Med Chem. Lett.* **18**, 2114–2121 (2008).
48. Krishna, M. T. et al. Inhibition of mast cell tryptase by inhaled APC 366 attenuates allergen-induced late-phase airway obstruction in asthma. *J. Allergy Clin. Immunol.* **107**, 1039–1045 (2001).
49. Ganesan, R., Eigenbrot, C. & Kirchhofer, D. Structural and mechanistic insight into how antibodies inhibit serine proteases. *Biochem J.* **430**, 179–189 (2010).
50. Maun, H. R. et al. Bivalent antibody pliers inhibit beta-tryptase by an allosteric mechanism dependent on the IgG hinge. *Nat. Commun.* **11**, 6435 (2020).
51. Rhee, H. et al. Airway tryptase levels inform the lack of clinical efficacy of the tryptase inhibitor MTPS9579A in asthma. *Allergy* **79**, 2993–3004 (2024).
52. Hartley, B. S. Homologies in serine proteinases. *Philos. Trans. R. Soc. Lond. B Biol. Sci.* **257**, 77–87 (1970).
53. Ereno-Orbea, J. et al. Structural basis of enhanced crystallizability induced by a molecular chaperone for antibody antigen-binding fragments. *J. Mol. Biol.* **430**, 322–336 (2018).
54. Huber, R. & Bode, W. Structural basis of the activation and action of trypsin. *Acc. Chem. Res* **11**, 114–122 (1978).
55. Cook, K. M., McNeil, H. P. & Hogg, P. J. Allosteric control of betaII-tryptase by a redox active disulfide bond. *J. Biol. Chem.* **288**, 34920–34929 (2013).
56. Bush-Pelc, L. A. et al. Important role of the cys-191 cys-220 disulfide bond in thrombin function and allostery. *J. Biol. Chem.* **282**, 27165–27170 (2007).
57. Miyata, T. et al. Coagulation factor XII (Hageman factor) Washington D.C.: inactive factor XIIa results from Cys-571–Ser substitution. *Proc. Natl. Acad. Sci. USA* **86**, 8319–8322 (1989).
58. Ganesan, R. et al. Unraveling the allosteric mechanism of serine protease inhibition by an antibody. *Structure* **17**, 1614–1624 (2009).
59. Schaefer, M., Buchmueller, A., Dittmer, F., Strassburger, J. & Wilmen, A. Allosteric inhibition as a new mode of action for BAY 1213790, a neutralizing antibody targeting the activated form of coagulation factor XI. *J. Mol. Biol.* **431**, 4817–4833 (2019).
60. Jiang, L. et al. Rezymogenation of active urokinase induced by an inhibitory antibody. *Biochem J.* **449**, 161–166 (2013).

61. Katschke, K. J. Jr. et al. Inhibiting alternative pathway complement activation by targeting the factor D exosite. *J. Biol. Chem.* **287**, 12886–12892 (2012).
62. Koschubs, T. et al. Allosteric antibody inhibition of human hepsin protease. *Biochem J.* **442**, 483–494 (2012).
63. Chavarria-Smith, J. et al. Dual antibody inhibition of KLK5 and KLK7 for Netherton syndrome and atopic dermatitis. *Sci. Transl. Med* **14**, eabp9159 (2022).
64. Mossner, E. et al. Increasing the efficacy of CD20 antibody therapy through the engineering of a new type II anti-CD20 antibody with enhanced direct and immune effector cell-mediated B-cell cytotoxicity. *Blood* **115**, 4393–4402 (2010).
65. Liang, W. C. et al. Dramatic activation of an antibody by a single amino acid change in framework. *Sci. Rep.* **11**, 22365 (2021).
66. Fu, Z., Akula, S., Thorpe, M. & Hellman, L. Highly selective cleavage of TH2-promoting cytokines by the human and the mouse mast cell tryptases, indicating a potent negative feedback loop on TH2 immunity. *Int. J. Mol. Sci.* **20**, 5147 (2019).
67. Gerhardy, S. et al. Allosteric inhibition of HTRA1 activity by a conformational lock mechanism to treat age-related macular degeneration. *Nat. Commun.* **13**, 5222 (2022).
68. Walters, B. T., Ricciuti, A., Mayne, L. & Englander, S. W. Minimizing back exchange in the hydrogen exchange-mass spectrometry experiment. *J. Am. Soc. Mass Spectrom.* **23**, 2132–2139 (2012).
69. Kan, Z. Y., Ye, X., Skinner, J. J., Mayne, L. & Englander, S. W. ExMS2: an Integrated Solution for Hydrogen-Deuterium Exchange Mass Spectrometry Data Analysis. *Anal. Chem.* **91**, 7474–7481 (2019).
70. Walters, B. T., Mayne, L., Hinshaw, J. R., Sosnick, T. R. & Englander, S. W. Folding of a large protein at high structural resolution. *Proc. Natl. Acad. Sci. USA* **110**, 18898–18903 (2013).
71. Walters, B. T. Empirical method to accurately determine peptide-averaged protection factors from hydrogen exchange MS data. *Anal. Chem.* **89**, 1049–1053 (2017).
72. Masson, G. R. et al. Recommendations for performing, interpreting and reporting hydrogen deuterium exchange mass spectrometry (HDX-MS) experiments. *Nat. Methods* **16**, 595–602 (2019).
73. Mastronarde, D. N. Automated electron microscope tomography using robust prediction of specimen movements. *J. Struct. Biol.* **152**, 36–51 (2005).
74. Iudin, A. et al. EMPIAR: the electron microscopy public image archive. *Nucleic Acids Res.* **51**, D1503–D1511 (2023).
75. Punjani, A., Rubinstein, J. L., Fleet, D. J. & Brubaker, M. A. cryoSPARC: algorithms for rapid unsupervised cryo-EM structure determination. *Nat. Methods* **14**, 290–296 (2017).
76. Goddard, T. D. et al. UCSF ChimeraX: meeting modern challenges in visualization and analysis. *Protein Sci.* **27**, 14–25 (2018).
77. Croll, T. I. ISOLDE: a physically realistic environment for model building into low-resolution electron-density maps. *Acta Crystallogr. D. Struct. Biol.* **74**, 519–530 (2018).
78. Afonine, P. V. et al. Real-space refinement in PHENIX for cryo-EM and crystallography. *Acta Crystallogr D. Struct. Biol.* **74**, 531–544 (2018).
79. The PyMOL Molecular Graphics System, Version 3.1.3 Schrödinger, LLC.

Acknowledgements

We thank the antibody production group and biomolecular resource group for respective antibody and tryptase expression and purification. We acknowledge Sigrid Noreng and Alberto Estevez for initial cryoEM work. We thank Anthony Kossiakoff for helpful discussions regarding the nanobody to bind Fab E104.v2 as a fiducial marker and assessing binding to a conformationally rigid active site. We thank Hong Li for outsourcing expression in mammalian constructs. We thank Daniel Kirchhofer for helpful comments and discussions on the manuscript. We thank Seth Harris for his help with zymogen modeling for Supplementary Movie 1.

Author contributions

H.R.M. and R.A.L. conceived the project. H.R.M. performed SEC experiments, generated and analyzed SDS-PAGE data, performed enzymatic activity assays and purified and characterized the complexes. A.M. and K.M.L. developed and performed the initial enzymatic activity assays. C.M.A. generated grids, collected and processed cryoEM data. C.M.A. and A.R. modeled and refined PDB coordinates. B.T.W. performed the HDX-MS experiments and analyzed the data. R.V., and J.T.K. carried out antibody engineering and binding kinetics. H.R.M., C.M.A. and R.A.L. interpreted the data and wrote the manuscript with input from all authors. H.R.M. and R.A.L. are co-senior authors.

Competing interests

All authors were employees of Genentech, Inc. and shareholders of Roche stock at the time the work was done.

Additional information

Supplementary information The online version contains supplementary material available at https://doi.org/10.1038/s41467-026-70491-3.

Correspondence and requests for materials should be addressed to Henry R. Maun or Robert A. Lazarus.

Peer review information *Nature Communications* thanks Daniel Kober, who co-reviewed with Pankaj Kumar; Lars Hellman; and Kasper Rand for their contribution to the peer review of this work. A peer review file is available.